

Energy equivalent model in analysis of postbuckling of imperfect carbon nanotubes resting on nonlinear elastic foundation

Nazira Mohamed^{1a}, Mohamed A. Eltahir^{*2,3}, Salwa A. Mohamed^{1b} and Laila F. Seddek^{1c}

¹Department of Engineering Mathematics, Faculty of Engineering, Zagazig University, P.O. Box 44519, Zagazig, Egypt

²Mechanical Engineering Dept., Faculty of Engineering, King Abdulaziz University, P.O. Box 80204, Jeddah, Saudi Arabia

³Mechanical Design & Production Dept., Faculty of Engineering, Zagazig University, P.O. Box 44519, Zagazig, Egypt

(Received June 26, 2018, Revised March 17, 2019, Accepted March 19, 2019)

Abstract. This paper investigates the static and dynamic behaviors of imperfect single walled carbon nanotube (SWCNT) modeled as a beam structure by using energy-equivalent model (EEM), for the first time. Based on EEM Young's modulus and Poisson's ratio for zigzag $(n, 0)$, and armchair (n, n) carbon nanotubes (CNTs) are presented as functions of orientation and force constants. Nonlinear Euler-Bernoulli assumptions are proposed considering mid-plane stretching to exhibit a large deformation and a small strain. To simulate the interaction of CNTs with the surrounding elastic medium, nonlinear elastic foundation with cubic nonlinearity and shearing layer are employed. The equation governed the motion of curved CNTs is a nonlinear integro-partial-differential equation. It is derived in terms of only the lateral displacement. The nonlinear integro-differential equation that governs the buckling of CNT is numerically solved using the differential integral quadrature method (DIQM) and Newton's method. The linear vibration problem around the static configurations is discretized using DIQM and then is solved as a linear eigenvalue problem. Numerical results are depicted to illustrate the influence of chirality angle and imperfection amplitude on static response, buckling load and dynamic behaviors of armchair and zigzag CNTs. Both, clamped-clamped (C-C) and simply supported (SS-SS) boundary conditions are examined. This model is helpful especially in mechanical design of NEMS manufactured from CNTs.

Keywords: differential integral quadrature method; curved carbon nanotube; energy equivalent model; static post-buckling instability; linear vibration

1. Introduction

Carbon nanotube (CNT) is a graphene layer rolled into tubular shape with a diameter around one nanometer and a length up to many micrometers, discovered in 1991 by Iijima. CNTs have received widespread interest of researchers due to their extraordinary mechanical, thermal, physical and electrical properties. CNTs are considered the strongest and most resilient material known until now, Eltahir *et al.* (2016). CNTs characteristics are controlled by two parameters, which are the orientation of the chiral angle and the carbon diameter.

The chiral vector used to describe the chiral angle, can be defined by

$$\vec{C}_h = n\vec{a}_1 + m\vec{a}_2 \quad (1)$$

where \vec{a}_1 and \vec{a}_2 are the unit vectors, and (n, m) is integer pair specifies the structure orientation of CNTs [i.e:

zigzag at $(n, 0)$, armchair at (n, n) , and chiral orientation at (n, m) for $m \neq n$ or 0] as shown in Figure 1. In 1995, Yamabe depicted the radius of nanotube as a function of integer pair (n, m) by

$$R = l_0 \sqrt{3(n^2 + m^2 + n * m)} / 2\pi \quad (2)$$

where l_0 is the C-C bond length ($=0.142 \text{ nm}$) and n is the translation index. Zigzag and armchair nanotubes radii are calculated by $R = \frac{\sqrt{3}na}{2\pi}$, and $R = \frac{3na}{2\pi}$, respectively.

Harik (2001 & 2002) proved that the structural characteristics of CNTs can be modelled as a beam for small radii and a cylindrical shell for large radii. Nasdala *et al.* (2012) illustrated that the standard truss and beam elements can be represented atomic interactions accurately. Energy equivalent model, resulting from the foundation of molecular and continuum mechanics, considers the mechanical properties of CNTs (i.e; Young's modulus, shear modulus, and Poisson's ratio) as a material size-dependent by many researchers. Li and Chou (2003) established a linkage between structural mechanics and molecular mechanics to model a deformation of CNTs act as beams. Leung *et al.* (2005) proposed a combined model of molecular and continuum mechanics to investigate mechanical properties of zigzag single walled carbon nanotubes (SWCNTs).

Wang *et al.* (2005) employed advanced finite element analysis package (ABAQUS) to obtain nonlinear bending

*Corresponding author, Professor

E-mail: meltaher@kau.edu.sa

^a Ph.D.

E-mail: naziramohamed@zu.edu.eg

^b Ph.D.

E-mail: sa_mohamed@zu.edu.eg

^c Ph.D.

E-mail: leseddek@zu.edu.eg

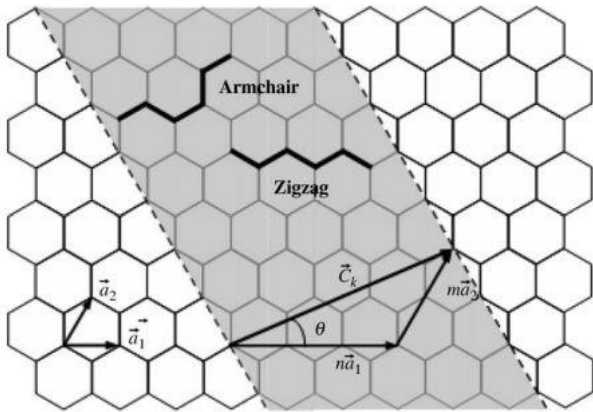


Fig 1. Schematic diagram of the chiral vector and the chiral angle of CNTs, Wu *et al.* (2006)

moment–curvature relationship of CNT. Wu *et al.* (2006) derived the equivalent Young and shear moduli for both armchair and zigzag SWCNTs by combining molecular and continuum mechanics methods. Hsieh *et al.* (2006) investigated the intrinsic thermal vibrations of a SWCNT modelled as a clamped cantilever beam. Cai *et al.* (2009) revealed experimentally and theoretically that Young's modulus of SWCNT varies in a wide range from 0.94 to 5.81 TPa. Shokrieh and Rafiee (2010) and Shodja and Delfani (2011) presented analytical formulations to predict the elastic moduli of graphene sheets and CNTs using a linkage between lattice molecular structure and equivalent discrete frame structure. Joshi *et al.* (2012) modeled the elastic behavior of CNTs reinforced composites by using the multiscale representative volume element approach. Le (2015) derived a closed-form expression for Young's modulus of hexagonal monolayer sheets based on molecular mechanics. Ghavamian and Ochsner (2015) investigated mechanical properties and mechanical behaviors of hetero-junction CNTs using finite element method. Ghadyani and Ochsner (2015) presented an expression for the stiffness of SWCNTs as function of nanotube thickness. Eltahir and Agwa (2016) presented a modified continuum energy equivalent model to investigate the vibration of a pretension CNTs carrying a concentrated mass as a mass sensor. Han *et al.* (2016) studied the influence of CNTs on the microstructure and ductility of CNT/Mg composites. Mohammadimehr and Alimirzaei (2016) investigated nonlinear static and vibration of Euler-Bernoulli functionally graded beam reinforced by carbon nanotubes with initial geometrical imperfection under uniformly distributed load using finite element method.

Tunneling Electron Microscope (TEM) images for carbon nanotubes (CNTs) illustrate that these tiny structures have a certain degree of curvature along the nanotubes length, Qian *et al.* (2000) and Wang *et al.* (2000). In 2007 Mikata derived an exact elastica solution for a clamped-hinged beam SWCNT by the elliptic integral technique. Mayoof and Hawwa (2009) investigated nonlinear vibration of CNT with waviness along its axis based on classical continuum theory. Mezghani *et al.* (2011) presented influence of carbon nanotube (CNT) on the mechanical properties of LLDPE/CNT nanocomposite fibers. Results

showed that, the small addition of CNT when properly mixed and aligned will increase the mechanical properties of pristine polymer fibers. Based on the nonlocal beam theory, Wang *et al.* (2012, 2013) studied the vibrations of simply supported double-walled CNTs subjected to a moving harmonic load by using nonlocal Euler and Timoshenko beam theories. Thongyothee and Chucheeprakul (2013) studied postbuckling behavior of curved nanorods including the effects of nonlocal elasticity theory and surface stress. Mohammadi *et al.* (2014) investigated the static instability of an imperfect nonlocal Eringen nanobeam embedded in elastic foundation. Khater *et al.* (2014) studied buckling behavior of curved nanowires including a surface energy under a thermal load.

Based on both material and size dependency, many researchers studied buckling and vibration behaviors of CNTs. Baghdadi *et al.* (2014) presented thermal effect on vibration of armchair and zigzag SWCNTs using nonlocal parabolic beam theory. Benguediab *et al.* (2014) studied buckling properties of a zigzag double-walled CNT with both chirality and small scale effects using Timoshenko beam. Semmah *et al.* (2015) presented the thermal buckling properties of a zigzag SWCNT based on the nonlocal Timoshenko beam and energy-equivalent model. Bedia *et al.* (2015) studied analytically thermal buckling of armchair SWCNT embedded in an elastic medium. On the basis of the continuum mechanics and the single-elastic beam model, Besseghier *et al.* (2015) investigated the nonlinear vibration of zigzag SWCNT embedded in elastic medium. Heshmati *et al.* (2015) studied the vibrational behavior of CNT-reinforced composite beams and presented the effects the interface, waviness, agglomeration, orientation and length on the behavior of CNTs. Farjam (2016) examined the pull-in behavior of a bio-mass sensor with a cantilevered CNT actuated electrostatically by taking into account rippling deformation. Galerkin-based reduced-order method was used to study the nonlinear structural behavior of actuated SWCNTs by Ouakad and Sedighi (2016). Eltahir *et al.* (2016) illustrated nonlinear static behavior of size-dependent and material-dependent nonlocal CNTs by using nonlocal differential form of Eringen and energy equivalent method. Hadji *et al.* (2016) developed a new higher order shear deformation model for static and free vibration analysis of functionally graded beams. Thermal postbuckling equilibrium paths of function graded CNT reinforced composite imperfect beams with various boundary conditions were studied by Wu *et al.* (2017). Free and forced vibrations of simply supported SWCNT under the influence of moving nanoparticle were analyzed by Salamat and Sedighi (2017). Sedighi and Farjam (2017) examined the dynamic pull-in instability of actuated cantilever CNT taking into account the rippling and charge concentration phenomena. Hadji *et al.* (2017 & 2018) presented a simple quasi-3D sinusoidal shear deformation theory with stretching effect for analyzing mechanical behaviors of carbon nanotube-reinforced composite beams resting on elastic foundation.

Kordkheili *et al.* (2018) employed nonlocal continuum theory of Eringen and Von Karman nonlinear strains to study a linear and nonlinear dynamics of SWNTs conveying fluid with different boundary conditions. Kadari *et al.* (2018)

presented the buckling of embedded orthotropic nanoplates by using a new hyperbolic plate theory and nonlocal small-scale effects. Eltaher *et al.* (2018) investigated analytically the vibration behavior of SWCNTs accompanying with the energy equivalent method and the modified couple stress. Mohamed *et al.* (2018) exploited differential-integral quadrature method to analyze nonlinear free and forced vibrations of buckled curved beams resting on nonlinear elastic foundations. Hamza-Cherif *et al.* (2018) investigated vibration of nano beam using differential transform method including thermal effect. Maneshi *et al.* (2018) presented closed-form expression for geometrically nonlinear large deformation of nano-beams subjected to end force. Emam *et al.* (2018) investigates the postbuckling and free vibration response of geometrically imperfect multilayer nanobeams under pre-stress compressive load. Torabi *et al.* (2019) studied buckling of different shapes of function graded CNT reinforced composite plates in thermal environment. Zouatnia and Hadji (2019) investigated effect of the micromechanical models on the bending of FGM beam using a new hyperbolic shear deformation theory. Eltaher *et al.* (2019a) investigated dynamical behaviors of perfect and defected C-C SWCNTs model as a beam structures by using finite element method. Eltaher *et al.* (2019b) exploited an energy equivalent model and finite element method to evaluate the equivalent Young's modulus of SWCNTs at any orientation angle by using tensile test.

According to the best of the authors' knowledge and literature review, it can be concluded that no researchers have attempted to investigate the postbuckling of curved CNTs by considering material size dependency. The present study is intended to fill this gap in the literature by considering the energy equivalent method along with nonlinear curved Euler-Bernoulli beam. This paper is organized as follows. Section 2 describes the mathematical formulation of the equivalent energy model for armchair and zigzag SWCNTs continuum. Main formulations and equations of motion for a nonlinear Euler-Bernoulli CNT with moderate rotation are presented. In Section 3, differential-integral quadrature method is presented and developed to solve a nonlinear integro-differential equation of material size dependent carbon nanotube. Numerical results are presented and discussed in Sections 4. Most findings and concluding remarks are summarized in Sections 5.

2. Mathematical formulation

2.1 Molecular Mechanics Effect

To establish a linkage between the microscopic chemistry and the macroscopic mechanics, covalent bonds between carbon atoms is represented by a force filed as a function of bond lengths and bond angles. The force filed can be represented by a potential energy as, [Rappé *et al.* (1992)]

$$PE = PE_L + PE_\theta + PE_T + PE_\omega \quad (3)$$

where PE_L , PE_θ , PE_T , and PE_ω are bond stretching, angle variation, torsion and inversion (out of plane) energies. When SWCNTs subjected to tension and bending loading in two-dimensional loading, bond stretching and

angle energies are the most significant and the other energies can be neglected. Therefore, Eq. (3) can be simplified as, Wu *et al.* (2006), Shokrieh and Rafiee (2010), Eltaher and Agwa (2016)

$$PE = PE_L + PE_\theta = \frac{1}{2} \sum_i K_i (dR_i)^2 + \frac{1}{2} \sum_j C_j (d\theta_j)^2 \quad (4)$$

where K_i is the stretching constant, dR_i is the elongation of the bond i , C_j is the angle variance constant, $d\theta_j$ is the variance of bond angle j .

For armchair orientation, Young's modulus and Poisson's ratio for CNTs can be described by [Wu *et al.* (2006), Bedia *et al.* (2015), Baghdadi *et al.* (2015)]

$$E_a = \frac{4\sqrt{3}}{3} \frac{KC}{Ct + 4Kl_0^2 t (\lambda_{a1}^2 + 2\lambda_{a2}^2)} \quad (5a)$$

$$\nu_a = \frac{\lambda_{a1} l_0^2 K - C}{\lambda_{a1} l_0^2 K + 3C} \quad (5b)$$

where t is the thickness of a nanotube, λ_{a1} and λ_{a2} are geometrical dependent parameters that given by

$$\lambda_{a1}(n) = \frac{4 - \cos^2(\pi/2n)}{16 + 2\cos^2(\pi/2n)} \quad (6a)$$

$$\lambda_{a2}(n) = \frac{-\sqrt{12 - 3\cos^2(\pi/2n)} \cos(\pi/2n)}{32 + 4\cos^2(\pi/2n)} \quad (6b)$$

However, Young's modulus and Poisson's ratio in case of Zigzag orientation, can be depicted by [Benguediab *et al.* (2014), Baghdadi *et al.* (2015), Besseghier *et al.* (2015), Eltaher *et al.* (2016)]:

$$E_z = \frac{4\sqrt{3}KC}{9Ct + 4Kl_0^2 t (\lambda_{z1}^2 + 2\lambda_{z2}^2)} \quad (7a)$$

$$\nu_a = \frac{\lambda_{z1} l_0^2 K + \sqrt{3}C}{\lambda_{z1} l_0^2 K - 3\sqrt{3}C} \quad (7b)$$

and geometrical dependent parameters in this case can be presented as

$$\lambda_{z1}(n) = \frac{-3\sqrt{4 - 3\cos^2(\pi/2n)} \cos(\pi/2n)}{8\sqrt{3} - 2\sqrt{3}\cos^2(\pi/2n)} \quad (8a)$$

$$\lambda_{z2}(n) = \frac{12 - 9\cos^2(\pi/2n)}{16\sqrt{3} - 4\sqrt{3}\cos^2(\pi/2n)} \quad (8b)$$

2.2 Problem Statement of Curved CNTs

The equilibrium equations of curved CNTs in lateral direction as a function of both axial and lateral deformations is presented in this section. Based on the kinematic Euler-Bernoulli beam assumptions, the axial displacement (U) and lateral deformation (W) of any generic point originally located at coordinates $(\hat{x}, 0, \hat{z})$ in the beam's undeformed state can be described as

$$U(\hat{x}, \hat{z}, \hat{t}) = \hat{u}(\hat{x}, \hat{t}) - \hat{z} \left[\frac{\partial \hat{w}}{\partial \hat{x}} - \frac{d\hat{w}_0}{d\hat{x}} \right] \quad (9a)$$

$$W(\hat{x}, \hat{z}, \hat{t}) = \hat{w}(\hat{x}, \hat{t}) \tag{9b}$$

in which \hat{u} and \hat{w} are the axial and transverse displacements along the neutral axis of the beam and \hat{w}_0 is the initial imperfection (initial rise) of the beam. The nonlinear axial strain including the moderate deformation assumption can be depicted by von Karman strain effect as follows:

$$\begin{aligned} \epsilon_x &= \frac{\partial U}{\partial \hat{x}} + \frac{1}{2} \left(\left(\frac{\partial W}{\partial \hat{x}} \right)^2 - \left(\frac{\partial \hat{w}_0}{\partial \hat{x}} \right)^2 \right) \\ &= \frac{\partial \hat{u}}{\partial \hat{x}} - \hat{z} \left(\frac{\partial^2 \hat{w}}{\partial \hat{x}^2} - \frac{d^2 \hat{w}_0}{d\hat{x}^2} \right) \\ &+ \frac{1}{2} \left(\left(\frac{\partial \hat{w}}{\partial \hat{x}} \right)^2 - \left(\frac{d\hat{w}_0}{d\hat{x}} \right)^2 \right) = \epsilon_0 + \hat{z}k_0 \end{aligned} \tag{10}$$

where normal and curvature strains at neutral axis of beam can be depicted by

$$\epsilon_0 = \frac{\partial \hat{u}}{\partial \hat{x}} + \frac{1}{2} \left(\left(\frac{\partial \hat{w}}{\partial \hat{x}} \right)^2 - \left(\frac{d\hat{w}_0}{d\hat{x}} \right)^2 \right) \tag{11a}$$

$$k_0 = - \left(\frac{\partial^2 \hat{w}}{\partial \hat{x}^2} - \frac{d^2 \hat{w}_0}{d\hat{x}^2} \right) \tag{11b}$$

and the force and moment resultants can be defined as

$$N = \frac{AE}{1 - \nu^2} \left[\frac{\partial \hat{u}}{\partial \hat{x}} + \frac{1}{2} \left(\left(\frac{\partial \hat{w}}{\partial \hat{x}} \right)^2 - \left(\frac{d\hat{w}_0}{d\hat{x}} \right)^2 \right) \right] \tag{10a}$$

$$M = \frac{-EI}{1 - \nu^2} \left[\left(\frac{\partial^2 \hat{w}}{\partial \hat{x}^2} - \frac{d^2 \hat{w}_0}{d\hat{x}^2} \right) \right] \tag{10b}$$

where A is the cross sectional area and I is the moment of inertia of CNT. The equations of motion of the CNTs with mid-plane stretching can be portrayed as

$$m \frac{\partial^2 \hat{u}}{\partial \hat{t}^2} - \frac{\partial N}{\partial \hat{x}} = \hat{F}_u \tag{13a}$$

$$m \frac{\partial^2 \hat{w}}{\partial \hat{t}^2} - \frac{\partial^2 M}{\partial \hat{x}^2} - N \frac{\partial^2 \hat{w}}{\partial \hat{x}^2} = \hat{F}_w \tag{13b}$$

in which $m = \int_A \rho dA$ is inertia term of CNTs. \hat{F}_u is the axial distributed force along the \hat{x} -axis and \hat{F}_w is the transverse force that simulates the nonlinear interaction of CNTs with the surrounding elastic medium. The transverse force can be illustrated by the following:

$$\hat{F}_w = -\bar{k}_L \hat{w} - \bar{k}_{NL} \hat{w}^3 + \bar{k}_s \frac{\partial^2 \hat{w}}{\partial \hat{x}^2} \tag{14}$$

where \bar{k}_L and \bar{k}_{NL} are linear and nonlinear elastic foundation coefficients, respectively, and \bar{k}_s is the shear stiffness of the elastic foundation. To reduce the governing equations into a single equation for the lateral deformation, the in-plane inertia and axial distributed forced are neglected. As a result, it can be concluded from Eq. (13a) that the induced axial force N is constant. Substituting Eq. (12) into Eq. (13), the following equations are obtained:

$$\frac{AE}{1 - \nu^2} \frac{\partial}{\partial \hat{x}} \left[\frac{\partial \hat{u}}{\partial \hat{x}} + \frac{1}{2} \left(\left(\frac{\partial \hat{w}}{\partial \hat{x}} \right)^2 - \left(\frac{d\hat{w}_0}{d\hat{x}} \right)^2 \right) \right] = 0 \tag{15a}$$

$$\begin{aligned} m \frac{\partial^2 \hat{w}}{\partial \hat{t}^2} + \frac{EI}{1 - \nu^2} \left[\left(\frac{\partial^4 \hat{w}}{\partial \hat{x}^4} - \frac{d^4 \hat{w}_0}{d\hat{x}^4} \right) \right] \\ - \frac{AE}{1 - \nu^2} \left[\frac{\partial \hat{u}}{\partial \hat{x}} \right] \\ + \frac{1}{2} \left(\left(\frac{\partial \hat{w}}{\partial \hat{x}} \right)^2 - \left(\frac{d\hat{w}_0}{d\hat{x}} \right)^2 \right) \left] \frac{\partial^2 \hat{w}}{\partial \hat{x}^2} = \hat{F}_w \end{aligned} \tag{15b}$$

By integrating Eq. (15a) with respect to spatial coordinate x , results

$$\frac{\partial \hat{u}}{\partial \hat{x}} = -\frac{1}{2} \left(\left(\frac{\partial \hat{w}}{\partial \hat{x}} \right)^2 - \left(\frac{d\hat{w}_0}{d\hat{x}} \right)^2 \right) - \frac{1 - \nu^2}{AE} c_1 \tag{16a}$$

$$\begin{aligned} \hat{u} = -\frac{1}{2} \int \left(\left(\frac{\partial \hat{w}}{\partial \hat{x}} \right)^2 - \left(\frac{d\hat{w}_0}{d\hat{x}} \right)^2 \right) d\hat{x} - \frac{1 - \nu^2}{AE} c_1 \hat{x} \\ + c_2 \end{aligned} \tag{16b}$$

Assuming that the CNT is constrained from movement at $\hat{x} = 0$, and the external compressive force \bar{P} is applied at $\hat{x} = L$. So that, the boundary conditions for the axial displacement \hat{u} are

$$\hat{u}(0) = 0 \quad \text{and} \quad \hat{u}(L) = \frac{-\bar{P}L(1-\nu^2)}{AE} \tag{17}$$

Calculating the constants of Eq. (16) by applying the boundary conditions given by Eq. (17), hence, Eq. (16a) can be presented as

$$\begin{aligned} \frac{\partial \hat{u}}{\partial \hat{x}} = -\frac{1}{2} \left(\left(\frac{\partial \hat{w}}{\partial \hat{x}} \right)^2 - \left(\frac{d\hat{w}_0}{d\hat{x}} \right)^2 \right) - \frac{\bar{P}(1 - \nu^2)}{AE} \\ + \frac{1}{2L} \int_0^L \left(\left(\frac{\partial \hat{w}}{\partial \hat{x}} \right)^2 - \left(\frac{d\hat{w}_0}{d\hat{x}} \right)^2 \right) d\hat{x} \end{aligned} \tag{18}$$

Substituting Eq. (18) into Eq. (15.b) yields the governing equation of motion of curved CNTs in terms of transverse displacement $\hat{w}(\hat{x}, \hat{t})$ as

$$\begin{aligned} m \frac{\partial^2 \hat{w}}{\partial \hat{t}^2} + \frac{EI}{1 - \nu^2} \left[\left(\frac{\partial^4 \hat{w}}{\partial \hat{x}^4} - \frac{d^4 \hat{w}_0}{d\hat{x}^4} \right) \right] \\ + \left[\bar{P} \right. \\ \left. - \frac{AE}{2L(1 - \nu^2)} \int_0^L \left(\left(\frac{\partial \hat{w}}{\partial \hat{x}} \right)^2 \right. \right. \\ \left. \left. - \left(\frac{d\hat{w}_0}{d\hat{x}} \right)^2 \right) d\hat{x} \right] \frac{\partial^2 \hat{w}}{\partial \hat{x}^2} = \hat{F}_w \end{aligned} \tag{19}$$

To evaluate the significance of the size parameter, orientation, and initial curvature on the resulting response, the following nondimensional parameters are introduced:

$$x = \frac{\hat{x}}{L}, \quad w = \frac{\hat{w}}{r}, \quad w_0 = \frac{\hat{w}_0}{r}, \quad r = \sqrt{\frac{I}{A}}, \tag{20}$$

$$t = \hat{t} \sqrt{\frac{EI}{(1-\nu^2)mL^4}}$$

As a result, the nondimensional equation of motion can be expressed by

$$\ddot{w} + w^{iv} + \left[P - \frac{1}{2} \int_0^1 (w'^2 - w_0'^2) dx \right] w'' + k_L w + k_{NL} w^3 - k_s w'' = w_0^{iv} \quad (21)$$

in which the nondimensional parameters can be represented by,

$$P = \frac{\bar{P}L^2(1-\nu^2)}{EI}, \quad k_L = \frac{L^4 \bar{k}_L(1-\nu^2)}{EI}, \quad k_{NL} = \frac{L^4 \bar{k}_{NL}(1-\nu^2)}{EA} \quad (22)$$

and $k_s = \frac{\bar{k}_s L^2(1-\nu^2)}{EI}$

subjected to the nondimensional boundary conditions

$$w = w' = 0 \text{ at } x = 0, 1 \quad (23a)$$

$$w = w'' = 0 \text{ at } x = 0, 1 \quad (23b)$$

For C-C and SS-SS CNTs respectively.

3. Solution Procedure

It is generally impossible to obtain analytical solution to the equation of motion (21). This difficulty is overcome by seeking approximate solutions. In this section, a differential-integral quadrature method (DIQM) is introduced. A detailed implementation in matrix form is described for static and linear vibration analyses.

3.1 Differential-integral quadrature method (DIQM)

The DIQM is a combination between integral quadrature method (IQM) and differential quadrature method (DQM).

a) Differential quadrature method (DQM)

In this method, the r -derivative of function $f(x)$ is approximated by

$$\frac{d^r}{dx^r} f(x) \Big|_{x=x_i} = \sum_{j=1}^{N_{dq}} \mathcal{M}_{ij}^{(r)} f(x_j), \quad i = 1, 2, \dots, N_{dq} \quad (24)$$

in which N_{dq} denotes the number of grid points discretized the domain of the problem, $0 \leq x \leq 1$, and $\mathcal{M}_{ij}^{(r)}$ is the weighting coefficients of the n^{th} -order derivatives. The weighting coefficients for the 1st-order derivatives can be given by Quan and Chang (1989)

$$\mathcal{M}_{ij}^{(1)} = \begin{cases} \frac{\mathcal{L}^{(1)}(x_i)}{(x_i - x_j)\mathcal{L}^{(1)}(x_j)} & i \neq j \\ - \sum_{j=1, j \neq i}^{N_x} \mathcal{M}_{ij}^{(1)} & i = j, \end{cases} \quad i, j = 1, 2, \dots, N_{dq} \quad (25)$$

where $\mathcal{L}^{(1)}(x)$ is defined as

$$\mathcal{L}^{(1)}(x) = \prod_{j=1, j \neq i}^{N_x} (x_i - x_j) \quad (26)$$

Introducing a column vector $f = [f(x_i)]^T = [f_1, f_2, \dots, f_{N_{dq}}]^T$, in which $f(x_i)$ is the nodal value of $f(x)$ at $x_i = \frac{1}{2} - \frac{1}{2} \cos\left(\frac{(i-1)\pi}{N_x-1}\right)$, $i = 1, 2, \dots, N_{dq}$. Also, let its first derivative vector will be $F^{(1)} = [F_1^{(1)}, F_2^{(1)}, \dots, F_{N_{dq}}^{(1)}]^T$, then a differential matrix operator of the first order derivative can be defined as

$$F^{(1)} = A^{(1)} f \quad (27)$$

where

$$A^{(1)} = [\mathcal{M}_{ij}^{(1)}], \quad i, j = 1, 2, \dots, N_{dq} \quad (28)$$

According to the DQM, the r^{th} -order derivative matrices are

$$A^{(r)} = [A^{(1)}]^r, \quad r > 1 \quad (29)$$

b) Integral quadrature method (IQM)

The IQM was introduced in Attia and Mohamed (2017) as a new method for computing numerical integration. This method is based on the DQM. In this method, an accurate row vector integral operator for definite integral is introduced. If we have a continuous function $f(x)$ in a domain $0 \leq x \leq 1$ and

$$\frac{df}{dx} = F(x) \quad (30)$$

Then

$$\int_0^x F(x) dx = f(x) - f(0) \quad (31)$$

Equation (30) is discretized in matrix form as Eq. (27) whose inverse is

$$f = [A^{(1)}]^{-1} F^{(1)} \quad (32)$$

However, matrix $A^{(1)}$ is singular and hence has no unique inverse. Mathematically this is expected since the anti-derivative of a given function is not unique due to the presence of the constant of integration. In this study the definite integral between two nodes x_i, x_j is considered. So, the inverse of matrix $A^{(1)}$ is computed using pseudo inverse algorithm. Consequently, the definite integral is computed as

$$\int_{x_i}^{x_j} F(x) dx = f(x_j) - f(x_i) \cong \sum_{k=1}^{N_{dq}} ([B]_{jk} - [B]_{ik}) F_k^{(1)} \quad (33)$$

where the symbol \cong stands for ‘‘is discretized or approximated by’’ and B is the pseudo-inverse of $A^{(1)}$. From Eq. (33), one can deduce that

$$\int_0^1 F(x) dx \cong \sum_{k=1}^{N_{dq}} ([B]_{N_{dq}k} - [B]_{1k}) F_k^{(1)} = R_{dq} F^{(1)} \quad (34)$$

in which the row vector R_{dq} is just the difference between

the last and first rows of the matrix B .

3.2 Static analysis

The static response of CNT is obtained by dropping the time dependent terms from Eq. (21). Then, the static response of imperfect CNTs in prebuckling and postbuckling states is given by

$$w_s^{iv} + \left[P - \frac{1}{2} \int_0^1 (w_s'^2 - w_0'^2) dx \right] w_s'' + k_L w_s + k_{NL} w_s^3 - k_s w_s'' = w_0^{iv} \quad (35)$$

subject to the following boundary conditions

$$\text{C-C:} \quad w_s = w_s' = 0 \text{ at } x = 0, 1 \quad (36a)$$

$$\text{SS-SS:} \quad w_s = w_s'' = 0 \text{ at } x = 0, 1 \quad (36b)$$

where w_s is the static deflected position due to applied axial load P . Following Nayfeh and Emam (2008), Eq. (35) can be simplified as

$$w_s^{iv} + \lambda^2 w_s'' + k_L w_s + k_{NL} w_s^3 = w_0^{iv} \quad (37a)$$

in which

$$\lambda^2 = P - k_s - \frac{1}{2} \int_0^1 (w_s'^2 - w_0'^2) dx \quad (37b)$$

A column vector w_s is defined as

$$w_s = [w_{s1}, w_{s2}, w_{s3}, \dots, w_{sN_{dq}}]^T \quad (38)$$

where $w_{si} = w_s(x_i)$. Upon using DIQM, Eq. (37a, b) are written as

$$A^{(4)} w_s + \lambda^2 A^{(2)} w_s + k_L w_s + k_{NL} w_s^{\circ 3} = A^{(4)} w_0 \quad (39a)$$

$$\lambda^2 = P - k_s - \frac{1}{2} R_{dq} [(A^{(1)} w_s)^{\circ 2} - (A^{(1)} w_0)^{\circ 2}] \quad (39b)$$

In discretization of Eq. (37) by DIQM, we used Hadamard p^{th} -power, defined for a vector V such that $V^{\circ p} = \{V_j^p\}$ and Hadamard product, defined for two matrices A, B as $A \circ B = [A_{ij} B_{ij}]$. In the same way, the boundary conditions can be given as

$$\begin{aligned} w_{s1} = w_{sN_{dq}} = 0, \quad \sum_{j=1}^{N_{dq}} [A^{(1)}]_{1j} w_{sj} \\ = 0, \quad \sum_{j=1}^{N_{dq}} [A^{(1)}]_{N_{dq}j} w_{sj} = 0 \end{aligned} \quad (40a)$$

For C-C CNTs, and

$$\begin{aligned} w_{s1} = w_{sN_{dq}} = 0, \quad \sum_{j=1}^{N_{dq}} [A^{(2)}]_{1j} w_{sj} \\ = 0, \quad \sum_{j=1}^{N_{dq}} [A^{(2)}]_{N_{dq}j} w_{sj} = 0 \end{aligned} \quad (40b)$$

For SS-SS CNTs. Equations of (39) form a system of $(N_{dq} + 1)$ nonlinear algebraic equations which can be rewritten as

$$G(w_s, \lambda^2) = 0 \quad (41)$$

Newton's iterative method is proposed to find a solution for Eq. (41). The Jacobian of this nonlinear system of equations can be given by

$$J = \begin{bmatrix} A^{(4)} + \lambda^2 A^{(2)} + k_L I_{N_{dq}} + 3k_{NL} D & A^{(2)} w_s \\ R_{dq} [(A w_s) O^T] \circ A & 1 \end{bmatrix} \quad (42)$$

where $I_{N_{dq}}$ is the identity matrix, O is column vector defined as $O = [O]_{N_{dq} \times 1} = [1, 1, 1, \dots, \dots, 1]^T$ and D is defined as

$$D = \begin{bmatrix} w_{s1}^2 & 0 & \dots & 0 \\ 0 & w_{s2}^2 & \dots & 0 \\ \vdots & \vdots & \dots & 0 \\ 0 & 0 & \dots & w_{sN_{dq}}^2 \end{bmatrix} \quad (43)$$

Note that, in Eqs. (41, 42) rows corresponding to boundaries are replaced by the corresponding boundary condition equations. Due to the nonlinearity in Eq. (39), it has multiple solutions. In fact, Eq. (39) has a unique solution if $P < P_c$ and three solutions if $P > P_c$. To compute the critical buckling load P_c , Eq. (39) is solved for certain axial load P with different initial guesses and check if the iteration converges to a unique solution or multiple solutions, where P_c is the load corresponding to the transition from one solution to three solutions.

4. Numerical results

The parameters used in the analysis of armchair and zigzag orientations of SWCNTs are: the effective thickness of CNTs $t=0.258$ nm, the forces constants $K/2= 46900$ kcal/mol/nm², and $C/2= 63$ kcal/mol/rad² [see Eltaher *et al.* (2016)], and the initial configuration of the curved CNT is assumed to be

$$w_0 = \begin{cases} \frac{1}{2} g [1 - \cos(2\pi x)] & \text{for C-C} \\ g \sin(\pi x) & \text{for SS-SS} \end{cases} \quad (50)$$

where g is the CNT mid span initial rise.

4.1 Validation

The applicability of the proposed numerical DIQM in solving the present nonlinear integro-differential equation is validated with analytical method presented by **Emam (2009)**. The buckling of Unidirectional laminate C-C beam with cosine type imperfection is solved. The dimensionless critical buckling loads are compared in **Table 1** with those obtained by **Emam (2009)**. Good agreement in results is noticed.

Table 1 Comparison of dimensionless critical buckling load of C-C unidirectional laminate beam, $k_L = k_{NL} = k_s = 0$

g	Present	Emam (2009)
0	39.4785	39.4784
1	66.6199	66.6198
2	76.6099	76.6099
3	78.8607	78.8606
4	74.6096	74.6095
5	64.3701	64.3701
6	48.4182	48.4181

Table 2 Critical buckling loads (nN) for C-C *armchair* and *zigzag* CNTs using DIQM, $L = 40nm$, $k_L = k_{NL} = k_s = 0$

g	<i>Armchair CNT</i>				<i>Zigzag CNT</i>			
	Armchair (5,5)	Armchair (10,10)	Armchair (15,15)	Armchair (20,20)	Zigzag (5,0)	Zigzag (10,0)	Zigzag (15,0)	Zigzag (20,0)
0	2.499903	12.31568	34.88008	75.55064	0.82409	3.340377	8.588337	17.60549
1	4.218428	20.78193	58.85793	127.4869	1.39060	5.636675	14.49227	29.70816
2	4.851002	23.89828	67.68397	146.6042	1.599128	6.481922	16.66546	34.16304
3	4.994107	24.60328	69.68066	150.9291	1.646302	6.673139	17.15709	35.17085
4	4.725627	23.28062	65.93467	142.8152	1.557381	6.312703	16.23039	33.27117
5	4.077223	20.08628	56.88776	123.2195	1.344052	5.447996	14.00717	28.71372
6	3.06599	15.10449	42.77846	92.65861	1.010700	4.096784	10.53311	21.59215
7	1.705228	8.40074	23.79232	51.53442	0.562126	2.27853	5.858255	12.00902
8	1.27e-06	6.24e-06	1.77e-05	3.83e-05	4.17e-07	1.69e-06	4.35e-06	8.92e-06
9	-2.04273	-10.0634	-28.5013	-61.7341	-0.67338	-2.7295	-7.01772	-14.3858

4.2 Static Results

4.2.1 Effect of imperfection amplitude on the critical buckling load

The effect of nondimensional imperfection amplitude on the critical buckling load for C-C and SS-SS CNTs is shown, respectively, in **Tables 2 and 3**. It is observed that, as the imperfection increases the buckling load is increased to a specific value and then decreased from a positive value (compressive force) to a negative one (tensile force). This phenomenon is consistent with the shell structure theories, **Srubshchik (1980)**. It is found that the critical buckling load of C-C CNTs nearly doubles as the normalized imperfection g reaches 3. The case where $g = 8$ yields the everted state where the CNT might buckle at zero load.

However, for SS-SS CNTs, as the imperfection amplitude increased from 0 to 2, the critical buckling load almost doubles. The everted state for SS-SS CNTs occurs when the imperfection amplitude g reaches 4. This is a characteristic of the onset of a peculiar system state which is known as a null-load equilibrium. It can also be noticed that the critical buckling load of both armchair and zigzag CNTs increases by increasing the chiral number. So that, the chiral number and the imperfection amplitude are significant parameters controlled critical buckling load of the CNTs. The same conclusions can be drawn from **Fig. 2** which presents effect of imperfection and chiral number on the critical buckling of C-C and SS-SS CNTs for both armchair and zigzag without any elastic foundation at $L = 40nm$.

4.2.2 Effect of imperfection amplitude on static response

Effects of nondimensional imperfection amplitude on the static response of C-C and SS-SS armchair and zigzag CNTs at $n = 15$ without any elastic foundation are illustrated in **Fig. 3**. In these figures, the solid lines are stable position and a dashed one is unstable position. It is noticed that, at a given chiral number, when the imperfection amplitude changes, the critical buckling load and the amplitude of static response are different. This means that the imperfection amplitude has a great influence on the static response of the curved CNTs.

4.2.3 Effect of chiral number on static response

Figure 4 illustrates the effects of chiral number on static response of armchair and zigzag CNTs with C-C and SS-SS boundary conditions at imperfection amplitude $g = 2$, length $L = 20 nm$ and without any elastic foundation. The convention of solid and dashed lines is the same as described in previous figures. It is observed that, the chiral number has a significant effect on the static response and can be used to enhance the CNTs function.

4.2.4 Effect of slenderness ratio on critical buckling load

The effect of slenderness ratio together with the imperfection amplitude on the critical buckling load of C-C and SS-SS CNTs for both armchair and zigzag is presented in **Table 4** and plotted in graphical form in **Fig. 5** for SS-SS

Table 3 Critical buckling loads (nN) for SS-SS *armchair* and *zigzag* CNTs using DIQM, $L = 40nm, k_L = k_{NL} = k_S = 0$

g	<i>Armchair CNT</i>				<i>Zigzag CNT</i>			
	Armchair (5,5)	Armchair (10,10)	Armchair (15,15)	Armchair (20,20)	Zigzag (5,0)	Zigzag (10,0)	Zigzag (15,0)	Zigzag (20,0)
0	0.62496	3.07883	8.71976	18.88709	0.20602	0.83507	2.14702	4.40124
0.5	1.05461	5.19548	14.71448	31.87173	0.34765	1.40917	3.62307	7.42704
1	1.21275	5.97457	16.92099	36.65106	0.39978	1.62048	4.16637	8.54076
1.5	1.24838	6.15010	17.41813	37.72786	0.41153	1.66809	4.28877	8.79169
2	1.18108	5.81857	16.47916	35.69404	0.38934	1.57817	4.05758	8.31775
2.5	1.01900	5.02004	14.21761	30.79550	0.33591	1.36158	3.50073	7.17625
3	0.76647	3.77600	10.69426	23.16389	0.25267	1.02416	2.63319	5.39786
3.5	0.42621	2.09969	5.94667	12.88054	0.14050	0.56950	1.46422	3.00154
4	0	0	0	0	0	0	0	0
4.5	-0.51085	-2.51670	-7.12771	-15.43870	-0.16840	-0.68260	-1.75502	-3.59767

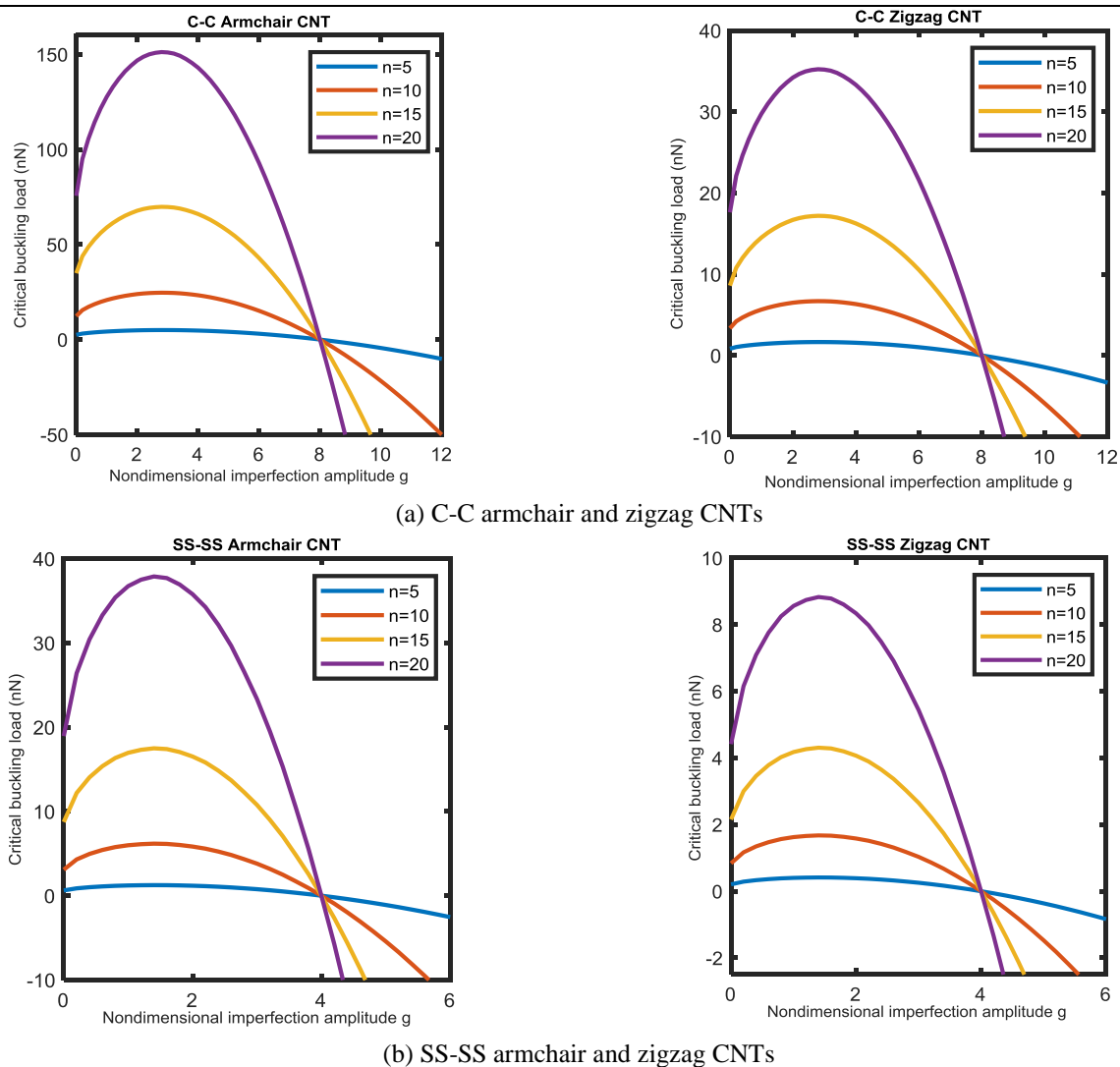


Fig. 2 Effect of imperfection amplitude on the critical buckling load

CNTs at chiral number $n = 14$ and without any elastic foundation. At a given imperfection amplitude, it is observed that, the critical buckling loads decrease rapidly as the slenderness ratio increases. This can be interpreted since increasing slenderness ratio decrease the rigidity of the

CNTs. This means that the slenderness ratio is a crucial parameter in determining the critical buckling load of the CNTs.

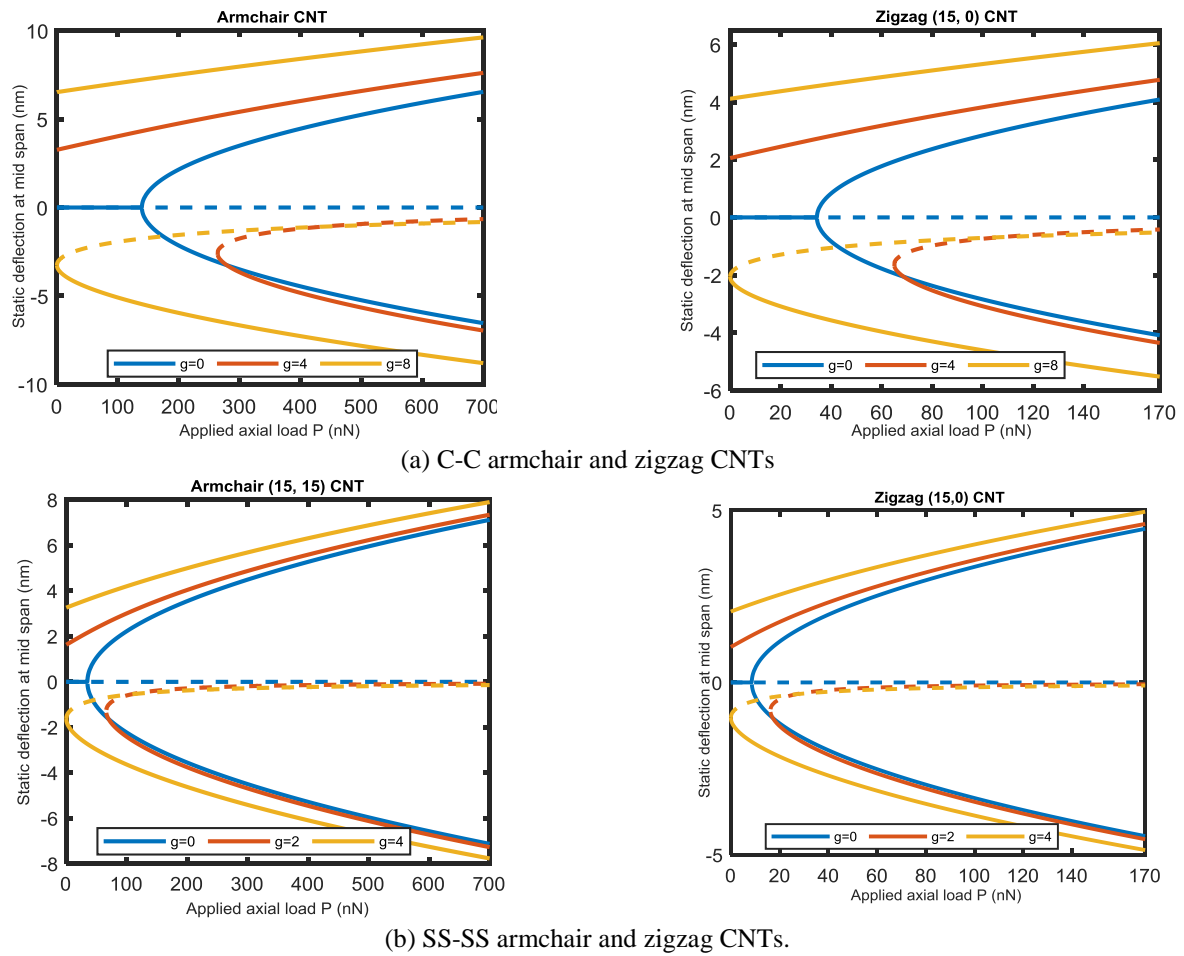


Fig. 3 Variation of the static response with the applied axial load of CNT at $n = 15$, $L = 20nm$ and $k_L = k_{NL} = k_s = 0$

Table 4 Effects of the slenderness ratio on the critical buckling load $P_c(nN)$ of C-C and SS-SS curved CNTs for both armchair and zigzag, $k_L = k_{NL} = k_s = 0$

CNT Type	L (nm)	L/D	C-C CNTs				SS-SS CNTs			
			$g = 0$	$g = 2$	$g = 3$	$g = 6$	$g = 0$	$g = 2$	$g = 3$	$g = 6$
<i>Armchair CNT</i>										
Armchair (14, 14)	10	5.2676	465.4420	903.1791	929.71330	570.8384	116.35696	219.89894	142.70489	-473.43868
	30	15.8028	51.7158	100.3532	103.30148	63.4265	12.92855	24.43322	15.85610	-52.60430
	50	26.3380	18.6177	36.1272	37.18853	22.8335	4.65428	8.79596	5.70820	-18.93755
	70	36.8732	9.4988	18.4322	18.97374	11.6498	2.37463	4.48773	2.91234	-9.66201
<i>Zigzag CNT</i>										
Zigzag (14, 0)	10	9.1237	116.3245	225.7249	232.35640	142.6654	29.08024	54.95772	35.66518	-118.32304
	30	27.3712	12.9249	25.0805	25.81738	15.8517	3.23114	6.10641	3.96280	-13.14700
	50	45.6187	4.6530	9.0290	9.29426	5.7066	1.16321	2.19831	1.42661	-4.73292
	70	63.8662	2.3740	4.6066	4.74197	2.9115	0.59347	1.12159	0.72786	-2.41476

4.2.5 Effects of the elastic foundation

The influence of the elastic foundation parameters on the critical buckling load of C-C CNTs for both armchair and zigzag are shown in Table 5. It can be observed that, an increase in the value of foundation parameters results in an increase in the buckling load for all CNTs. Furthermore, one can note that the nonlinear elastic foundation coefficient has no effect on the buckling load for perfect CNTs ($g = 0$).

Fig 6 shows the mutual effects of elastic foundation constants on the critical buckling load of SS-SS armchair and zigzag CNTs at chiral number $n = 10$, imperfection amplitude $g = 1$ and length $L = 40nm$. It is observed that with the increase in the shear foundation parameter, the buckling load of CNTs increases considerably. However, it is slightly increased with increasing the value of linear and nonlinear foundation parameters.

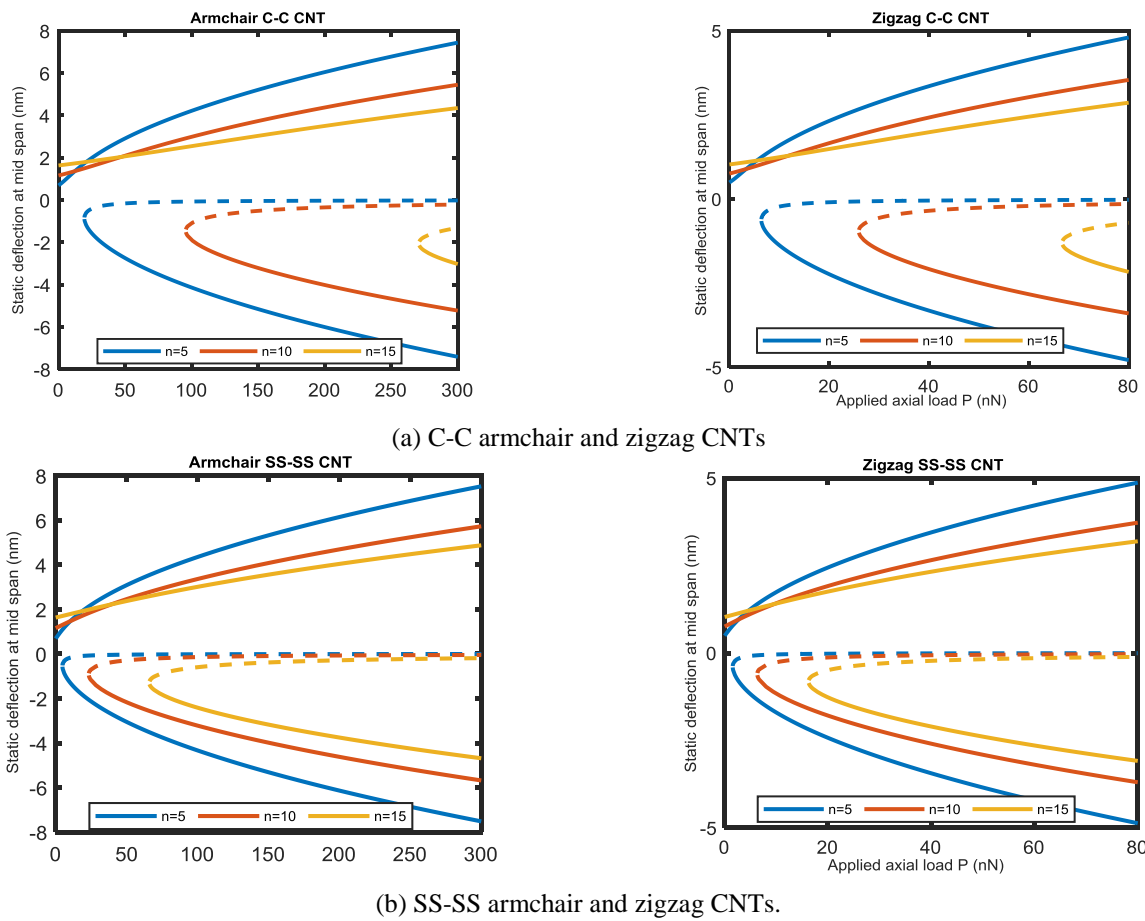


Fig. 4 Variation of the static response with the applied axial load of CNT at $g = 2$, $L = 20nm$ and $k_L = k_{NL} = k_s = 0$

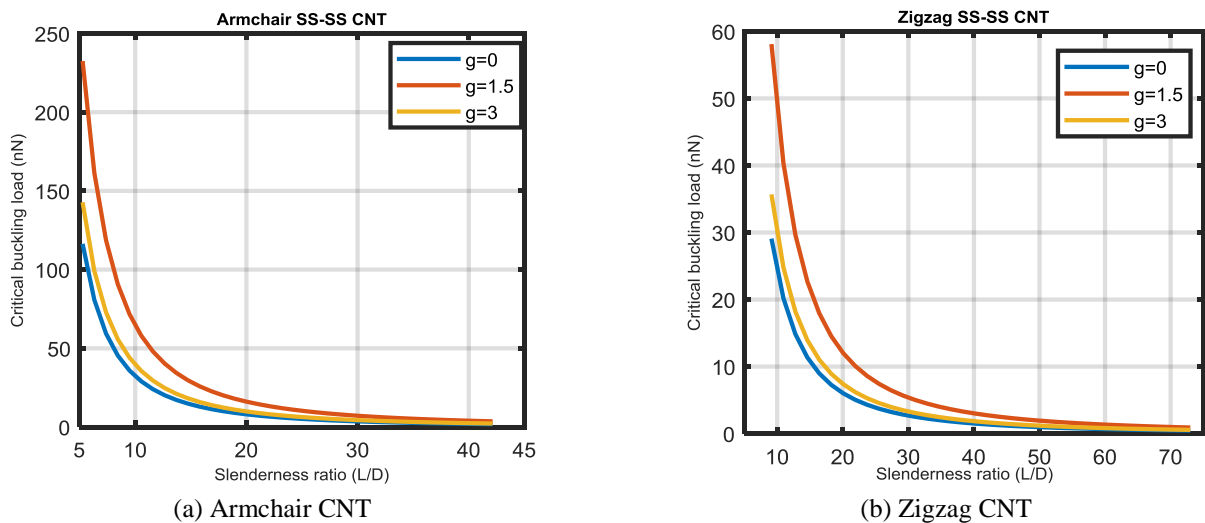


Fig. 5 effect of slenderness ratio on the critical buckling load of SS-SS armchair and zigzag CNTs for at $n = 14$ and $k_L = k_{NL} = k_s = 0$

4.3 Linear vibration results

In this section, the linear vibration of curved CNTs in prebuckling and postbuckling states is investigated. The variations of the first three natural frequencies of the upper and lower stable branches of SS-SS and C-C CNTs with the

applied axial load are illustrated in Fig. 7 when $g = 1$, $L = 20nm$ and $n = 15$. Solid line indicates 1st vibration frequency, dashed one indicates 2nd vibration frequency and dotted line indicates 3rd one. It is noticed that, as the applied load increases, the fundamental frequency around the upper branch decreases and then increases monotonically. In

Table 5 Effects of elastic foundations on critical buckling loads (nN) of C-C armchair and zigzag CNTs using DIQM, $L = 40nm$.

CNTs type	g	$(k_L, k_{NL}) = (0,0)$			$(k_s, k_{NL}) = (0,0)$			$(k_s, k_L) = (0,0)$		
		$k_s = 5$	$k_s = 10$	$k_s = 20$	$k_L = 5$	$k_L = 10$	$k_L = 20$	$k_{NL} = 5$	$k_{NL}=10$	$k_{NL} = 20$
Armchair (7, 7)	0	5.90562	6.56917	7.896278	5.289843	5.340273	5.441133	5.23941	5.23941	5.239413
	1	9.515347	10.1789	11.50601	8.891608	8.942038	9.042898	8.98317	9.11588	9.356095
	2	10.84245	11.5060	12.83311	10.21739	10.26782	10.36868	10.3925	10.6009	10.98047
	3	11.13442	11.7979	13.12507	10.51731	10.56641	10.66728	10.7601	11.0322	11.52591
	4	10.57703	11.24058	12.56769	9.951965	10.0077	10.10326	10.2572	10.5863	11.17954
zigzag (14, 0)	0	8.19472	9.11547	10.957	7.340258	7.410235	7.55019	7.27028	7.27028	7.27028
	1	13.2036	14.1244	15.9659	12.33812	12.40809	12.54805	12.46518	12.64933	12.98264
	2	15.0451	15.9659	17.8074	14.17778	14.24776	14.38772	14.42086	14.70998	15.23665
	3	15.4503	16.371	18.2125	14.59396	14.6621	14.80206	14.93096	15.30847	15.99351
	4	14.6768	15.5976	17.4391	13.80948	13.88683	14.01941	14.23303	14.68972	15.51288

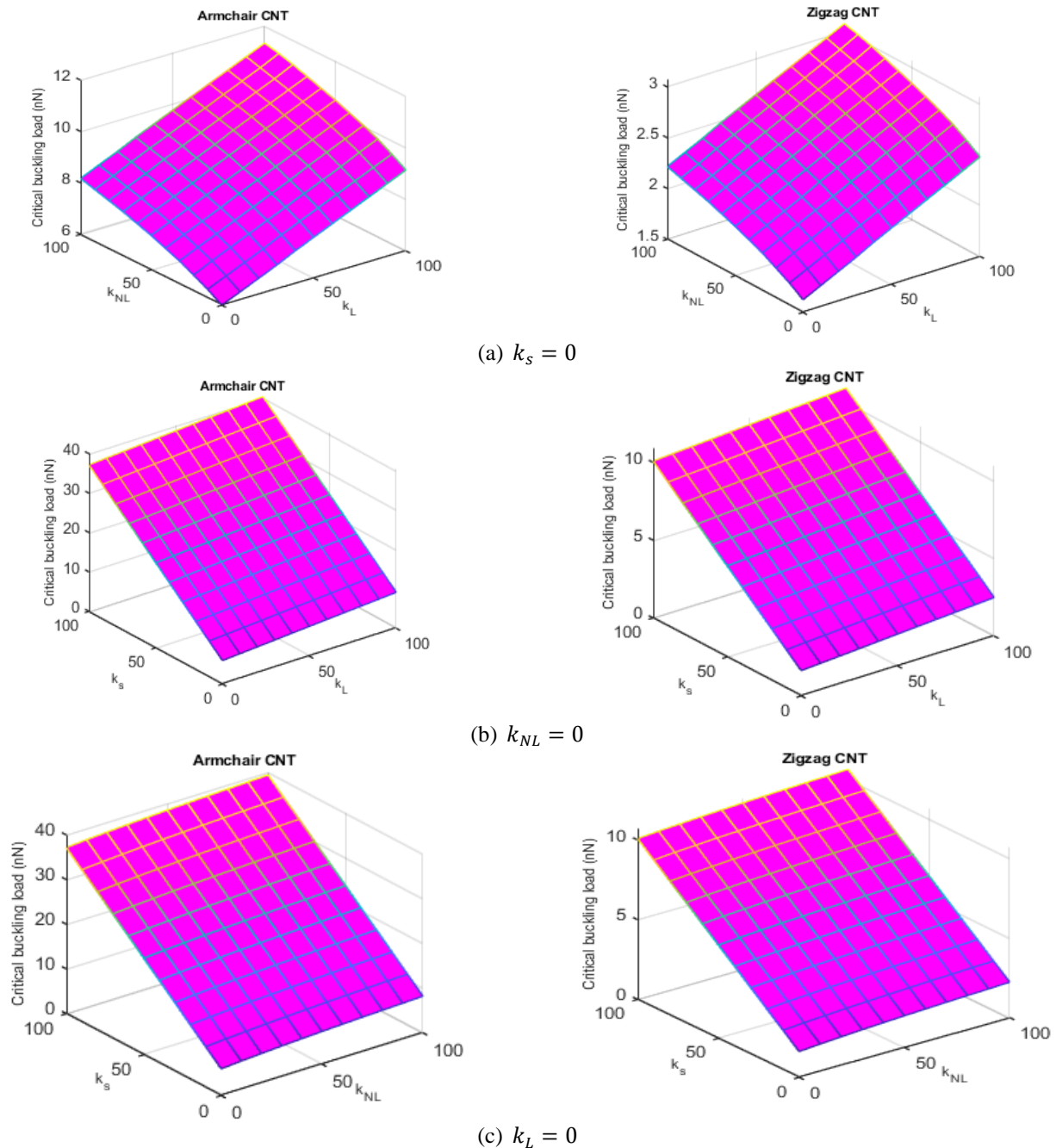


Fig. 6 Effect of elastic foundations on critical buckling load of SS-SS CNTs at $g = 1$, $L = 40nm$ and $n = 10$

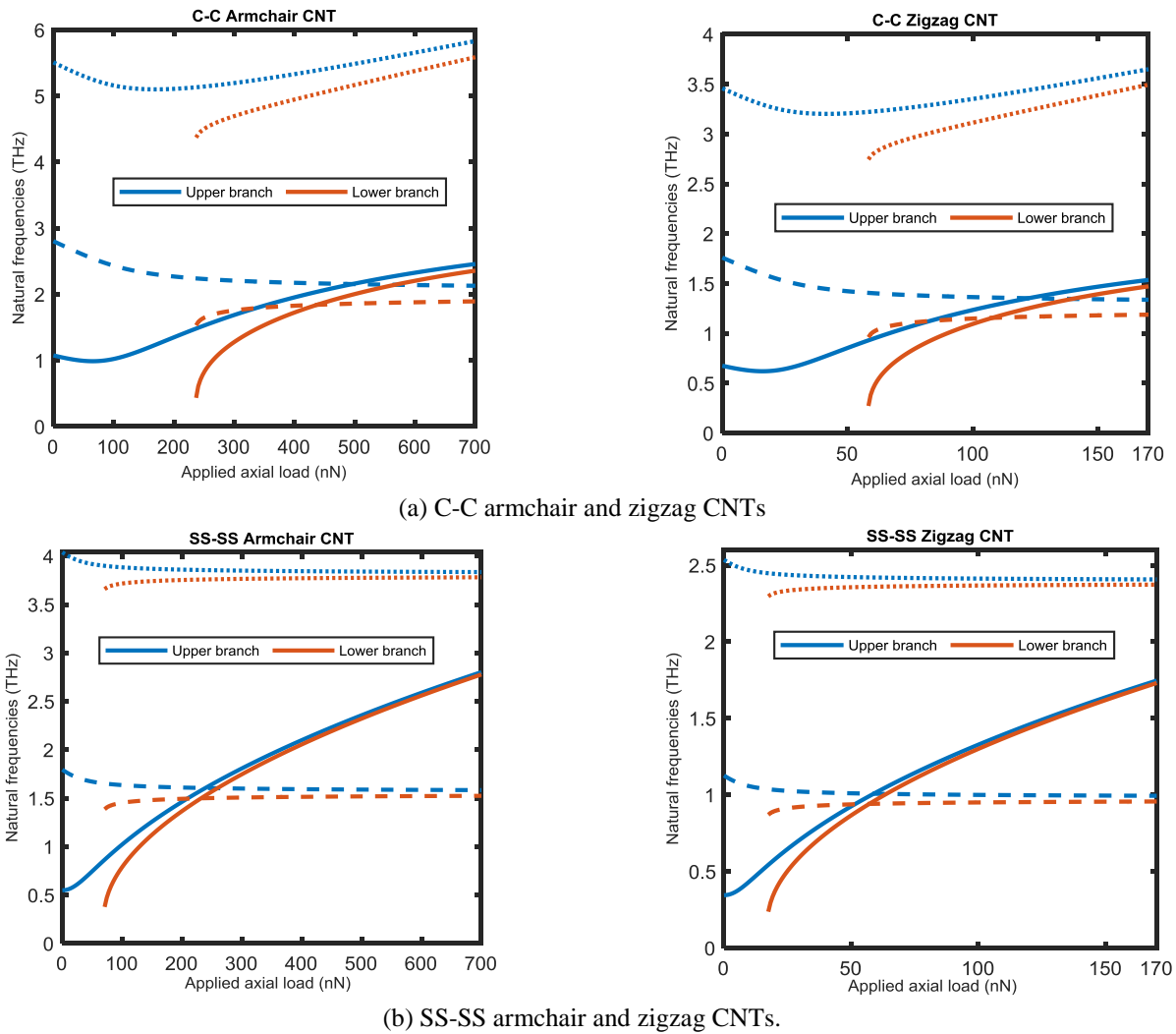


Fig. 7 Variation of the natural frequencies of the first three vibration modes with the applied axial load of C-C and SS-SS CNTs when $g = 1$, $L = 20\text{nm}$, $n = 15$ and $k_L = k_{NL} = k_s = 0$

contrast, around the lower branch, it increases monotonically with increasing the applied axial load.

Figure 8 shows the variation of the fundamental frequency of C-C and SS-SS curved CNTs for both armchair and zigzag at different values of chiral numbers. Here, only the frequencies associated with the upper branch are considered. The figures illustrate the significant effect of the chiral number on the first natural frequency.

5. Conclusions

Buckling, postbuckling configurations and dynamic behaviors around buckled position of C-C and SS-SS curved SWCNT for both armchair and zigzag resting on nonlinear elastic medium were numerically investigated. The DIQM with the Newton's iterative method were proposed to determine the buckling load and postbuckling equilibrium path of the CNTs. The convergence and accuracy of the present method were investigated by comparing the results with those available in the literature.

Numerical results show that the currently proposed DIQM has excellent stability and can achieve high

The effects of the imperfection amplitude, chiral number, slenderness ratio and elastic foundation parameters on buckling load, the postbuckling configurations and linear vibration of CNTs were discussed in detail. It was found that the critical buckling load and the lateral deflection of CNTs can be significantly enhanced by manipulating the imperfection amplitude. The critical buckling load could be doubled provided that a proper imperfection is employed. Also, it was concluded that increasing the elastic foundation parameters, the critical buckling load increases. Moreover, the buckling load and amplitude of static response increase by increasing the chiral number of CNTs. It is also noted that, the armchair orientation is stiffer than the zigzag orientation of CNTs. Furthermore, it was noticed that the chiral number has a great influence on the fundamental frequency of CNTs

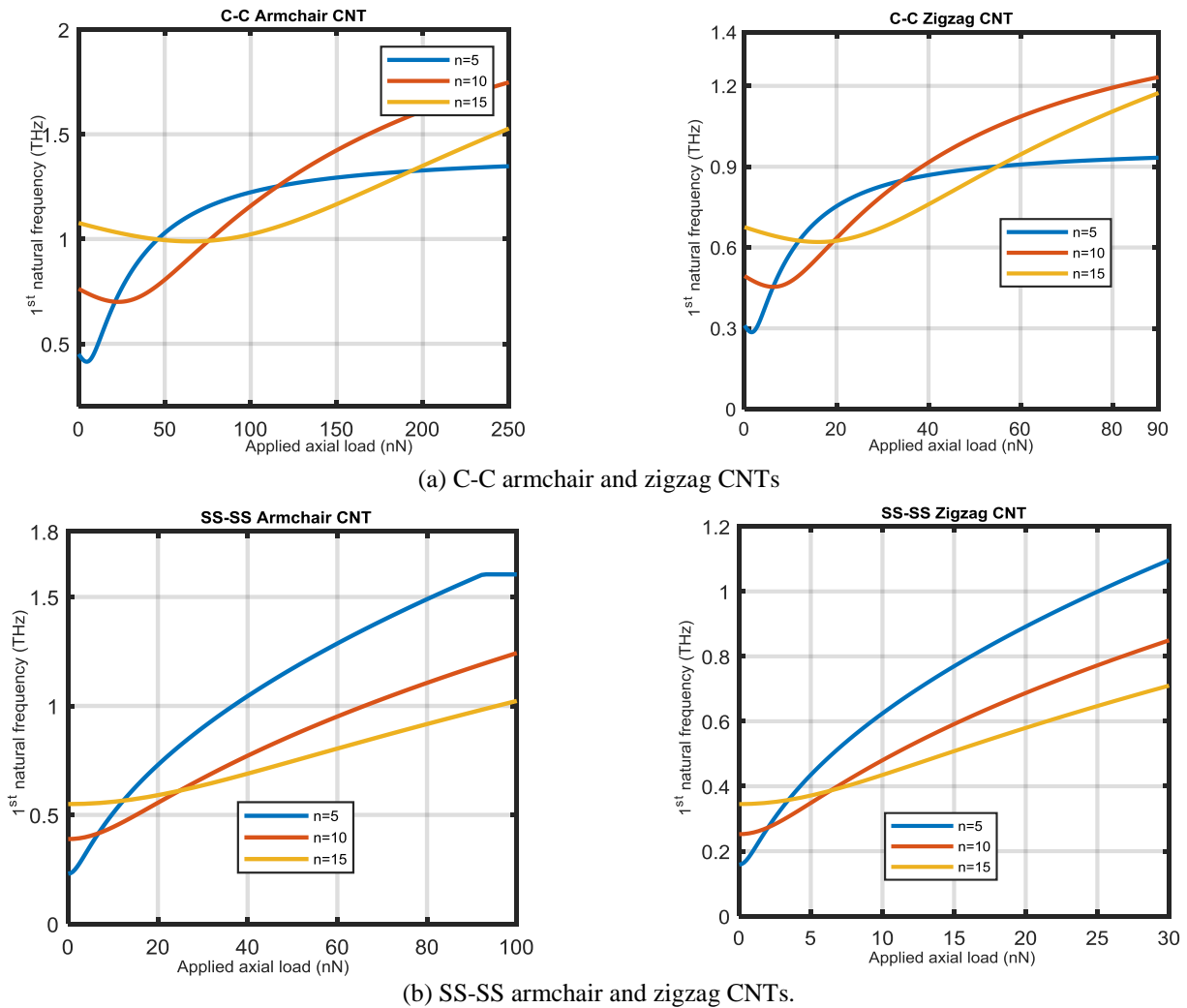


Fig. 8 Variation of the fundamental frequency of curved CNTs with the applied axial load when $g = 1$, $L = 20 \text{ nm}$ and $k_L = k_{NL} = k_s = 0$

References

- Attia M.A. and Mohamed S.A. (2017), "Nonlinear modeling and analysis of electrically actuated viscoelastic microbeams based on the modified couple stress theory", *Appl. Math. Model.*, **41**, 195-222. <https://doi.org/10.1016/j.apm.2016.08.036>.
- Baghdadi, H., Tounsi, A., Zidour, M. and Benzair, A. (2014), "Thermal effect on vibration characteristics of armchair and zigzag single-walled carbon nanotubes using nonlocal parabolic beam theory", *Fullerenes Nanotubes Carbon Nanostruct.*, **23**(3), 266-272. <https://doi.org/10.1080/1536383X.2013.787605>.
- Bedia, W.A., Benzair, A., Semmah, A., Tounsi, A. and Mahmoud, S.R. (2015), "On the thermal buckling characteristics of armchair single-walled carbon nanotube embedded in an elastic medium based on nonlocal continuum elasticity", *Brazilian J. Phys.*, **45**(2), 225-233. <https://doi.org/10.1007/s13538-015-0306-2>.
- Bellman, R. and Casti, J. (1971), "Differential quadrature and long-term integration", *J. Math. Anal. Appl.*, **34**(2), 235-238.
- Benguediab, S., Tounsi, A., Zidour, M. and Semmah, A. (2014), "Chirality and scale effects on mechanical buckling properties of zigzag double-walled carbon nanotubes", *Compos. Part B*, **57**, 21-24. <https://doi.org/10.1016/j.compositesb.2013.08.020>.
- Besseglier, A., Heireche, H., Bousahla, A.A., Tounsi, A. and Benzair, A. (2015), "Nonlinear vibration properties of a zigzag single-walled carbon nanotube embedded in a polymer matrix", *Adv. Nano Res.*, **3**(1), 029. <http://doi.org/10.12989/anr.2015.3.1.029>.
- Cai, J., Wang, C.Y., Yu, T. and Yu, S. (2009), "Wall thickness of single-walled carbon nanotubes and its Young's modulus", *Physica Scripta*, **79**(2), 025702.
- Eltaher, M.A. and Agwa, M.A. (2016), "Analysis of size-dependent mechanical properties of CNTs mass sensor using energy equivalent model", *Sensors Actuators A*, **246**, 9-17. <https://doi.org/10.1016/j.sna.2016.05.009>.
- Eltaher, M.A., El-Borgi S. and Reddy J.N. (2016), "Nonlinear analysis of size-dependent and material-dependent nonlocal CNTs", *Compos. Struct.*, **153**, 902-913. <https://doi.org/10.1016/j.compstruct.2016.07.013>.
- Eltaher, M.A., Agwa, M. and Kabeel, A. (2018), "Vibration Analysis of Material Size-Dependent CNTs Using Energy Equivalent Model", *J. Appl. Comput. Mech.*, **4**, 75-86. <https://dx.doi.org/10.22055/jacm.2017.22579.1136>.
- Eltaher, M.A., Almalki, T.A., Almitani, K.H., Ahmed, K.I.E. and Abdraboh, A.M. (2019a), "Modal participation of fixed-fixed single-walled carbon nanotube with vacancies", *J. Adv. Struct. Eng.*, 1-13. <https://doi.org/10.1007/s40091-019-0222-8>.
- Eltaher, M.A., Almalki, T.A., Ahmed, K.I. and Almitani, K.H. (2019b), "Characterization and behaviors of single walled

- carbon nanotube by equivalent continuum mechanics approach”, *Adv. Nano Res.*, **7**(1), 39-49. <https://doi.org/10.12989/anr.2019.7.1.039>.
- Emam, S.A. (2009), “A static and dynamic analysis of the postbuckling of geometrically imperfect composite beams”, *Compos. Struct.*, **90**(2), 247-253. <https://doi.org/10.1016/j.compstruct.2009.03.020>.
- Emam, S.A., Eltahir, M.A., Khater, M.E. and Abdalla, W.S. (2018), “Postbuckling and Free Vibration of Multilayer Imperfect Nanobeams under a Pre-Stress Load”, *Appl. Sci.*, **8**(11), 2238. <https://doi.org/10.3390/app8112238>.
- Farjam, N. (2016), “Pull-in behavior of a bio-mass sensor based on an electrostatically actuated cantilevered CNT with consideration of rippling effect”, *J. Appl. Comput. Mech.*, **1**(4), 229-239. <https://dx.doi.org/10.22055/jacm.2016.12006>.
- Ghadyani, G. and Öchsner, A. (2015), “On a thickness free expression for the stiffness of carbon nanotubes”, *Solid State Communications*, **209**, 38-44. <https://doi.org/10.1016/j.ssc.2015.03.004>.
- Ghavamian, A. and Öchsner, A. (2015), “A comprehensive numerical investigation on the mechanical properties of hetero-junction carbon nanotubes”, *Communications Theoretical Phys.*, **64**(2), 215.
- Hadji, L., Khelifa, Z., & El Abbes, A. B. (2016), “A new higher order shear deformation model for functionally graded beams”, *KSCE Journal of Civil Engineering*, **20**(5), 1835-1841. <https://doi.org/10.1007/s12205-015-0252-0>.
- Hadji, L., Zouatnia, N., Meziane, M.A.A. and Kassoul, A. (2017), “A simple quasi-3D sinusoidal shear deformation theory with stretching effect for carbon nanotube-reinforced composite beams resting on elastic foundation”, *Earthq. Struct.*, **13**(5), 509-518.
- Hadji, L., Meziane, M.A.A. and Safa, A. (2018), “A new quasi-3D higher shear deformation theory for vibration of functionally graded carbon nanotube-reinforced composite beams resting on elastic foundation”, *Struct. Eng. Mech.*, **66**(6), 771-781. <https://doi.org/10.12989/sem.2018.66.6.771>.
- Hamza-Cherif, R., Meradjah, M., Zidour, M., Tounsi, A., Belmahi, S. and Bensattalah, T. (2018), “Vibration analysis of nano beam using differential transform method including thermal effect”, *J. Nano Res.*, **54**, 1-14. <https://doi.org/10.4028/www.scientific.net/JNanoR.54.1>.
- Han, G.Q., Shen, J.H., Ye, X.X., Chen, B., Imai, H., Kondoh, K. and Du, W.B. (2016), “The influence of CNTs on the microstructure and ductility of CNT/Mg composites”, *Mater. Lett.*, **181**, 300-304. <https://doi.org/10.1016/j.matlet.2016.06.021>.